Materials Research Express

PAPER

Precipitate evolution during severe plastic deformation of cast Al-Zn-Mg alloys and their thermal stability

Materials Research Express

PAPER

Precipitate evolution during severe plastic deformation of cast Al-Zn-Mg alloys and their thermal stability

RECEIVED
8 August 2018

REVISED
10 September 2018

ACCEPTED FOR PUBLICATION
19 September 2018

PUBLISHED
10 October 2018

G K Manjunath, Prashant Huilgol, G V Preetham Kumar and K Udaya Bhat[1]

Department of Metallurgical & Materials Engineering, National Institute of Technology Karnataka, Surathkal, Mangalore–575025, India
[1] Author to whom any correspondence should be addressed.

E-mail: manjugk2001@gmail.com, prashanthuilgol@gmail.com, pkphd@hotmail.com and udayabhatk@gmail.com

Keywords: SPD, ECAP, Al-Zn-Mg alloy, TEM, precipitates, DSC

Supplementary material for this article is available online

Abstract

In the current investigation, an effort was made to understand the precipitate evolution process during equal channel angular pressing (ECAP) of an alloy composed of only aluminium, zinc and magnesium. For this purpose, three different compositions of cast Al-Zn-Mg alloys were selected and ECAP processed in route B_C upto four passes. Microstructural observations indicated that, ECAP processing leads to refined structure possessing high density dislocations and large amount of grains with high angle grain boundaries. The precipitate volume in the alloys increased with increase in the zinc quantity in the alloy. Microstructural characterization through transmission electron microscope (TEM) and differential scanning calorimeter (DSC) revealed that, processing by ECAP results in structure having stable η phase precipitates without the presence of GP zones and intermediate η' phase precipitates. Thereby demonstrates that, ECAP process accelerates the precipitation kinetics and also shifts the morphology of the precipitates. Higher mechanical properties were noticed in the alloy containing large quantity of $MgZn_2$ precipitates.

1. Introduction

Al-Zn-Mg alloys possess high toughness and also exhibit highest strength among all aluminium alloys. [1]. Al-Zn-Mg alloys are key engineering materials for the application in the automotive and the aerospace parts due to their high strength, high toughness and low density [1]. Also, these alloys have good specific strength and damage tolerance behaviour [2]. But these alloys possess less strength and poor ductility in cast condition restricts its engineering applications. In order to cater the increasing demand of these alloys in engineering field, study of these alloys is necessary. Strength of these alloys could be improved by various techniques like heat treatment, adding alloying and rare-earth elements, and coating techniques. These processes have various limitations like, not all properties will be improved in heat treatment process, adding alloying and rare-earth elements into the material changes composition and phases of the alloy system, only surface properties could be improved in coating techniques. Compared to these techniques strengthening via grain refinement is more attractive because of its number of benefits like simplicity in operation, cost effective, development of homogenous structure and properties throughout the material and no special equipments are needed for processing. Grain refinement could be accomplished via various severe plastic deformation (SPD) techniques. In SPD techniques, higher degree of grain refinement could be achieved through the application of the intensive plastic deformation. Also, processing via SPD techniques results in high angle grain boundaries [3]. Among several SPD techniques, equal channel angular pressing (ECAP) technique is the most effective and superior tool for the grain refinement [4]. ECAP was first invented in 1972 by Segal in Russia, later during early 1990s ECAP process gained a lot of interest to develop ultrafine and nanostructured materials [5]. Processing via ECAP will have positive effect on the precipitation and microstructure evolution in the materials. Also, ECAP processing at higher temperature promotes precipitation kinetics [6].

Table 1. Composition (in wt %) of the alloys with designations used in the present study.

Alloy	Designation	Aluminium	Zinc	Magnesium
Al-5Zn-2Mg	A5	93	5	2
Al-10Zn-2Mg	A10	88	10	2
Al-15Zn-2Mg	A15	83	15	2

Numerous literatures were stated to examine the importance of ECAP processing on Al-Zn-Mg alloys. Majority of the literature is on the wrought Al-Zn-Mg [7–9]. Generally, in wrought Al-Zn-Mg alloys, along with magnesium and zinc, other elements (Cu & Zr) are present, which leads to the growth of different sets of precipitates (like $MgZn_2$, Al_3Zr and Al_2Cu). It is hard to recognize the effect of each precipitate on the hardness and strength of the alloy. It is very essential to recognize the effect of each precipitate on the hardness and strength of the alloy. In this regard, in the present work, alloys composed of only aluminium, zinc and magnesium was studied. In this combination only Mg-Zn based precipitate formation takes place. Formation of other types of precipitates which are generally observed in commercial wrought alloys are eliminated. Also, very few literatures were reported to examine the importance of the SPD and other metal forming processes on cast alloys composed of only aluminium, zinc and magnesium [10–12]. The present work is motivated by the realization that, no literatures were reported to identify the precipitate evolution process involved in an alloy compiled of only aluminium, zinc and magnesium and processed through ECAP technique.

Along with that, it is very much essential to understand the thermal behaviour of the ECAP processed Al-Zn-Mg alloys. But, very few studies were reported on differential scanning calorimeter (DSC) analysis of Al-Zn-Mg alloys. Xu *et al* used DSC to determine the melting temperature of the Al 7034 alloy [13]. DeIasi and Adler studied the endothermic and exothermic reactions occurring in Al 7075 alloy and reported the dissolution and formation of the precipitates in the temperature between 20 to 500 °C [14]. Starink and Li developed a model to predict the electrical conductivity of the age-hardened Al-Zn-Mg-Cu alloy through DSC studies [15]. Starink and Wang developed a model to predict the yield strength of the age-hardened Al-Zn-Mg-Cu alloy through DSC studies [16]. To the author's knowledge, no literatures were found on the thermal stability of a cast alloy complied of only aluminium, magnesium and zinc and processed through ECAP technique. In the present work, Al-Zn-Mg alloys with variable zinc was selected and ECAP processed to study the effect of the zinc content on the evolution of Mg-Zn based precipitates, their thermal stability and mechanical properties.

In the present study, three different zinc compositions were selected (5, 10 and 15%). Even though, zinc could be added upto 40% to aluminium [17], increase in the zinc content above 20% leads to decrease in the ductility of the material [18, 19]. Also, zinc content less than 5% will not have significant influence on the expected properties of the alloy [17]. Hence, in the present work, zinc content is fixed minimum as 5% and maximum as 15%. The maximum solubility of magnesium in aluminium is 17.4%, for optimum mechanical properties the magnesium content should not be more than 4% [17]. Hence in the present study, zinc content is limited to 5, 10 and 15% and magnesium content is limited to 2%. The zinc and magnesium ratios are chosen such that it is susceptible to precipitation of $MgZn_2$ precipitates. By this study, effect of zinc content and ECAP processing on the microstructure, mechanical properties and thermal response of particular composition of aluminium, zinc and magnesium could be identified and utilized to suitable applications, since Al-Zn-Mg alloys are key engineering materials for the application in the automotive and aerospace parts [1]. From the results, it is noticed that, ECAP processing leads to increase in the mechanical properties of the alloys. Also, with increase in the zinc content, increase in the mechanical properties of the alloys is observed, suggesting that the studied alloys could be used as alternative materials for automotive and aerospace parts.

2. Experimental procedure

Table 1 shows the alloy composition studied in the present work. These alloys were initially prepared as cast ingots by gravity casting method. Casting was carried out in an electric resistance furnace. Initially, graphite crucible was kept inside the resistance furnace and crucible is heated to the melting temperature of the alloy. Afterwards, commercial pure aluminium (99.7% purity) pieces of required quantity were poured into the crucible. Once, the aluminium pieces were melted, zinc (99.9% purity) granules and magnesium (99.9% purity) granules covered in the aluminium foils were poured to the aluminium melt and stirred manually using a graphite rod. After that, melt was degassed with hexachloroethylene tablets. Later, the melt was cast into cylindrical rods of 25 mm diameter and 100 mm length using a metal die. Homogenization of the cast ingots was taken place at 480 °C for 20 h. For ECAP, homogenized alloys were machined to 16 mm diameter and 80 mm length rods.

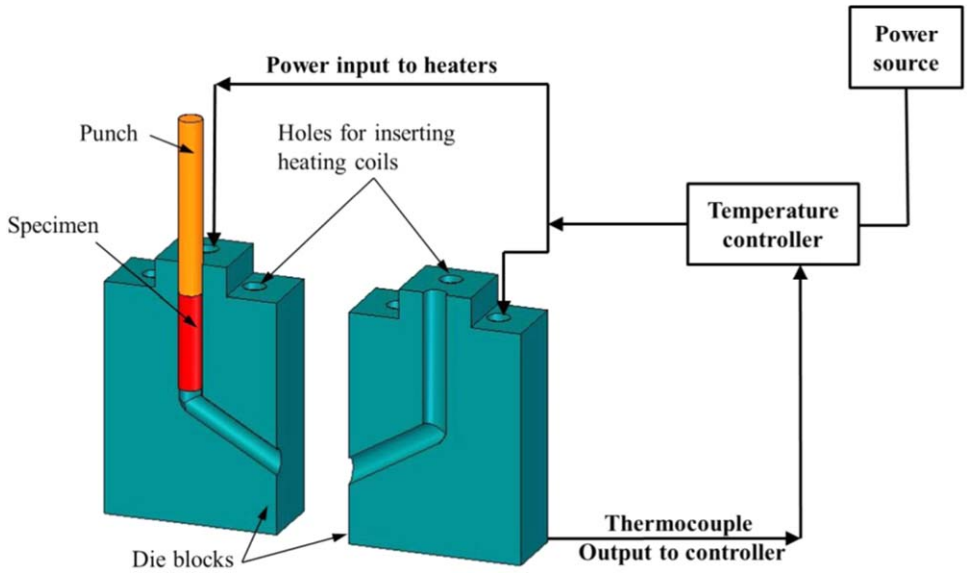

Figure 1. Schematic showing the temperature control during processing.

The ECAP processing was taken place in a split die, the die channels are intersecting at an angle (Φ) of 120° and outer arc of curvature (Ψ) of 30°. With these angles, in each pass, a stain of 0.667 is imposed on the sample. In the present work samples were processed though route B_C. All three alloy samples were tried to process at lowest possible temperature. The least temperature at which all three alloys were fruitfully processed upto four number of passes in route B_C, without crack is 200 °C. After 4 passes, pressing was stopped. Since, in route B_C, deformation restores the equiaxed microstructure in all 3 planes after each 4 consecutive passes [20]. Pressing was taken place at a speed of 0.5 mm s^{-1}. Molybdenum disulphide was applied on the specimen and the die channel to control friction during processing. A separate heating arrangement was used for heating the die assembly to the required processing temperature. Figure 1 shows the schematic diagram of the heating arrangement used in the present study. Die blocks were heated by using heating coils. Holes were drilled in the die to insert the heating coils as shown in figure 1. These coils were controlled by temperature controller. To measure the temperature in the die, thermocouple was used and this thermocouple sends signal (temperature rise in the die) to the controller. In this way, controller controls the required temperature in the die during processing.

Microstructure of the processed and unprocessed materials was studied by using Zeiss AX10 LAB A1 optical microscope (OM) and Jeol JEM-2100 transmission electron microscope (TEM). For OM study, specimens were prepared by metallographic techniques. For TEM study, specimens were thinned down to 80 μm thickness and 3 mm diameter discs were pierced from the thinned specimens. The pierced specimen is further thinned down to 40 μm thickness using disc polisher. The specimens were then dimpled to 20 μm thickness using dimple grinder. Ion milling of the dimpled specimens were carried out at 4° beam angle until perforation was achieved. These samples were studied in TEM and selected area electron diffraction (SAED) patterns were recorded. TEM with energy dispersive spectroscopy (EDS) was used to analyse the chemical composition. Thermal analysis of the processed and unprocessed materials were carried out in Netzsch 404 F1 differential scanning calorimeter (DSC). For DSC study, specimens of 5 mm diameter with approximate weight of 20 mg were sealed in aluminium pans and heated in argon atmosphere at a constant heating rate of 10 °C min^{-1}. DSC curves were recorded over a temperature 100 to 600 °C.

To assess the mechanical properties of the processed and unprocessed materials, microhardness measurement and tensile test experiments were conducted at room temperature. Microhardness measurements were carried out in Shimadzu HMV-G20 ST microhardness indenter. Microhardness measurements were conducted at a load of 50 gm for 15 s. In cast and homogenized samples microhardness was measured perpendicular to the ingot axis. While in the ECAP processed samples, microhardness was measured perpendicular to the processing direction. In each condition, ten measurements were conducted and average values were considered. Tensile tests were conducted in Shimadzu AG–X plus 100 kN universal testing machine according to ASTM E8 standard. For tensile testing, samples were machined to tensile test samples as per the ASTM E8 standard (gauge length = 24 mm, gauge diameter = 6 mm). Cast and homogenized samples were machined parallel to the ingot axis, while the ECAP processed samples were machined parallel to the processed

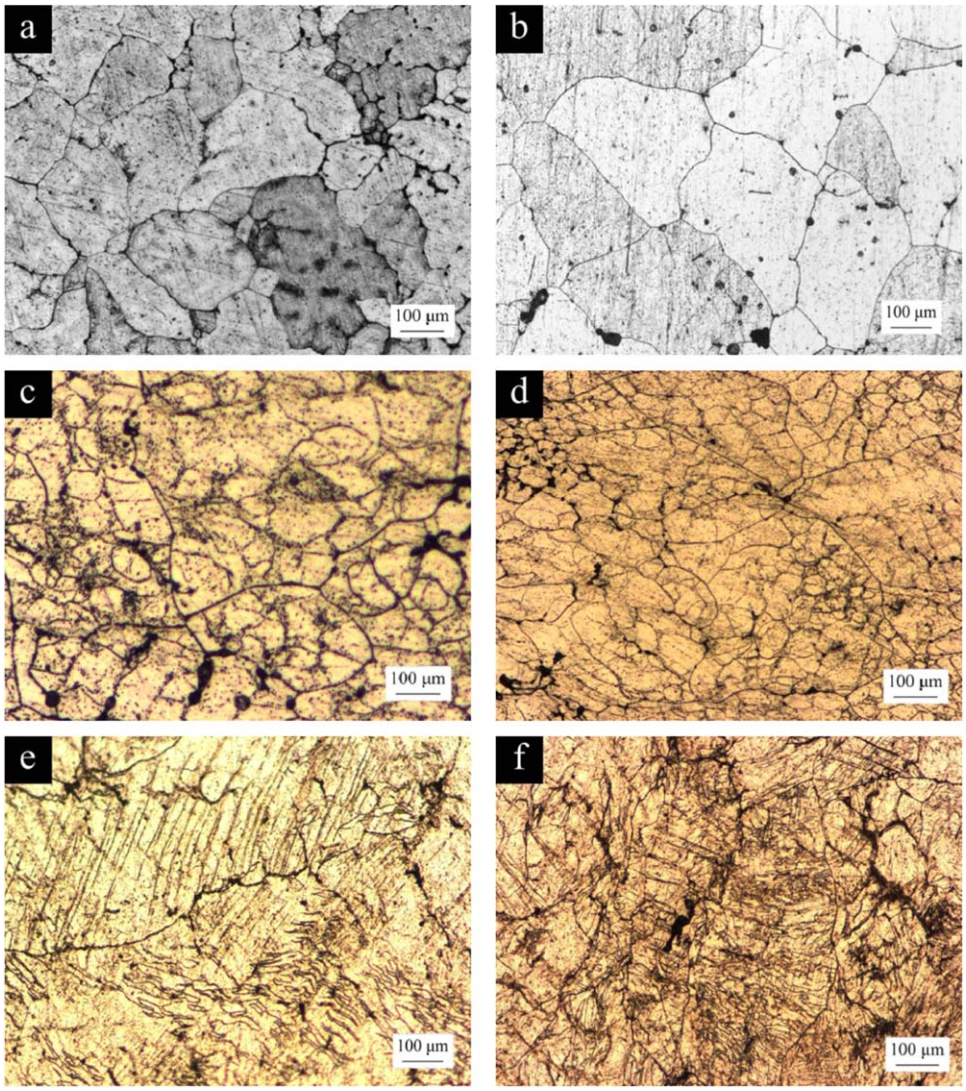

Figure 2. OM micrographs of the A5 alloy in different conditions (a) cast, (b) homogenized, (c) 1 pass, (d) 2 pass, (e) 3 pass and (f) 4 pass.

direction. Tensile tests were conducted at a constant cross head speed of 0.1 mm min^{-1}. In each condition, three samples were tested to confirm the repeatability of the results and average values were considered.

3. Results

3.1. Optical microscope (OM)

Figure 2 presents the OM micrographs of the A5 alloy in various conditions. In cast condition, dendritic structure was observed and precipitates were identified in the dendrites, as displayed in figure 2(a). In this condition, dendrites in the size range of 150 to 200 μm were observed. After homogenization treatment, due to the recrystallization, grains were identified as displayed in figure 2(b) and precipitates were almost dissolved in the matrix. In homogenized condition, grains in the size range of 180 to 200 μm were observed. It is noticed that, processing by ECAP leads to significant reduction in the grain size of the alloy. After first pass, microstructure was refined by the introduction of the sub-grains as displayed in figure 2(c). In this condition, grains in the size of 30 to 50 μm were observed. After second pass, due to the formation of new sub grains, more refined grain structure was observed compared to previous pass, as shown in figure 2(d). In this condition, grains in the size range of 20 to 30 μm were observed. Figure 2(e) shows the OM micrograph of the alloy after third pass. In this condition, large amount of shear bands were observed within the large initial grains and newly generated sub-grains. After third pass, size of the shear bands varies from 10 to 15 μm. After fourth pass, grain structure was refined to a great extent as shown in figure 2(f). Finer size shear bands were noticed compared to previous pass. After fourth pass, size of the shear band varies from 5 to 8 μm.

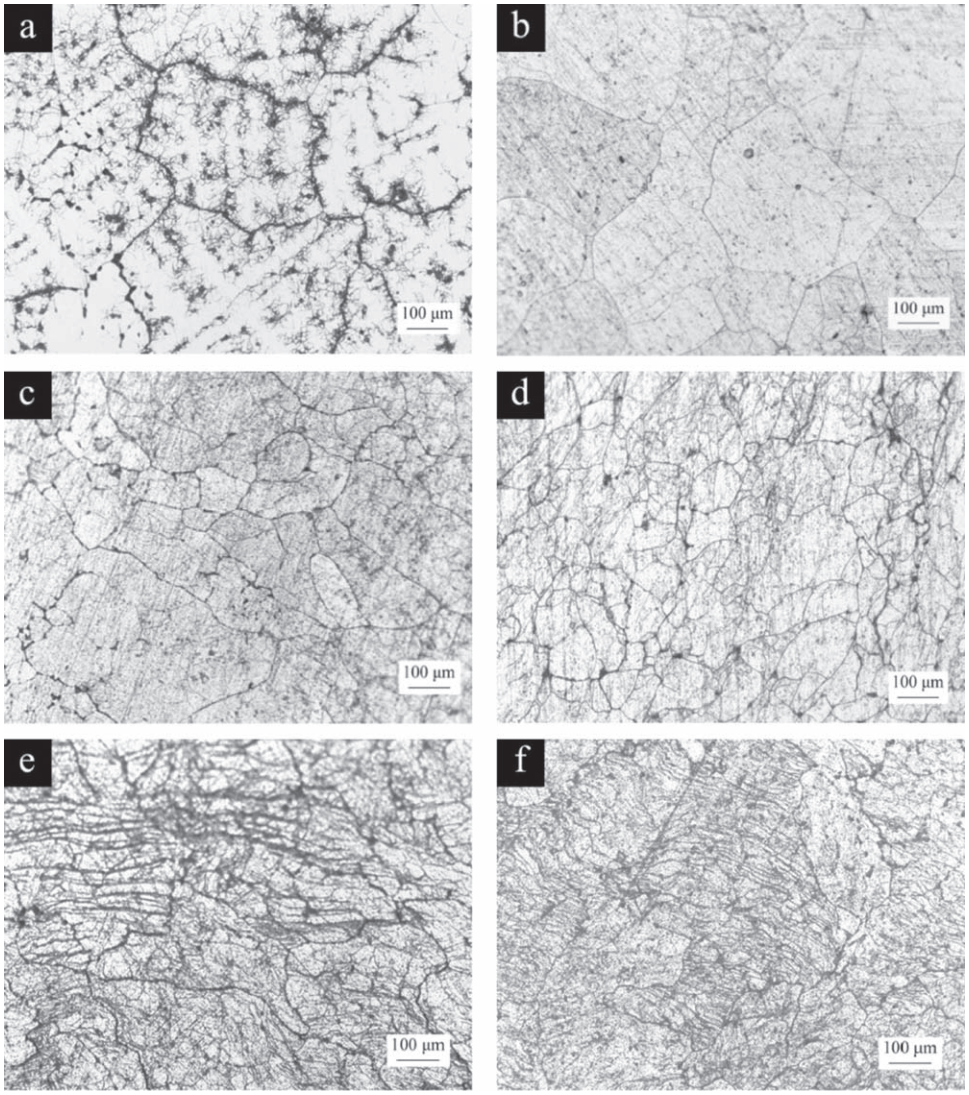

Figure 3. OM micrographs of the A10 alloy in different conditions (a) cast, (b) homogenized, (c) 1 pass, (d) 2 pass, (e) 3 pass and (f) 4 pass.

Figure 3 displays the OM micrographs of the A10 alloy in different conditions. In cast condition, dendrites in the size range of 240 to 280 μm were observed as shown in figure 3(a) and precipitates were identified in the dendrites. After homogenization treatment, grains in the size of 200 to 240 μm were identified as shown in figure 3(b). The grain structure of the alloy was refined significantly after ECAP processing. In the first pass, grain size of the alloy was reduced to 70 to 90 μm as shown in figure 3(c). After second pass, grain size of the alloy was reduced to 40 to 50 μm as shown in figure 3(d). After third pass, large amount of shear bands were observed within the large initial grains and newly generated sub-grains as shown in figure 3(e). The size of the shear bands measured in this condition is approximately equal to 20 μm. After fourth pass, more refined shear bands in the size of 10 μm were observed as shown in figure 3(f).

Figure 4 shows the OM micrographs of the A15 alloy in different conditions. In cast condition, large size dendrites in the range of 160 to 200 μm were observed as shown in figure 4(a). After homogenization, large size grains in the range of 120 to 180 μm were observed as shown in figure 4(b). After ECAP, significant reduction in the grain size of the alloy was observed. Figure 4(c) shows the microstructure of the alloy after first pass. The size of the grains measured in this condition is approximately equal to 40 μm. After second pass, grain size of the alloy was reduced to 25 μm as shown in figure 4(d). After third pass, grain size measured in the alloy is approximately equal to 15 μm as shown in figure 4(e). After fourth pass, grain size measured in the alloy is approximately equal to 10 μm as shown in figure 4(f).

3.2. Transmission electron microscope (TEM)

Figure 5 presents the TEM micrographs and associated SAED patterns of the A5 alloy in various conditions. In cast condition, dendritic structure with minimum number of dislocations was observed. The discrete spots in

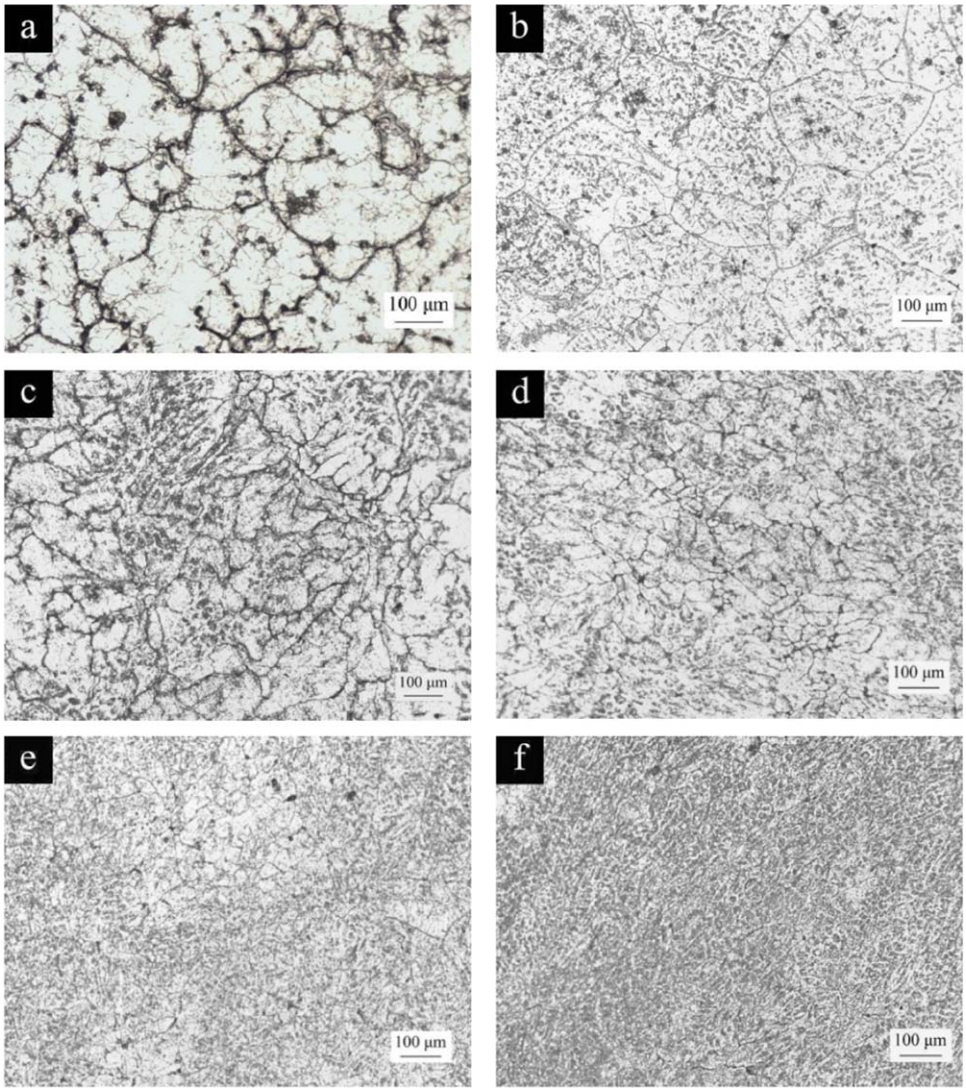

Figure 4. OM micrographs of the A15 alloy in different conditions (a) cast, (b) homogenized, (c) 1 pass, (d) 2 pass, (e) 3 pass and (f) 4 pass.

the SAED pattern are due to coarse dendrites (pattern is from one of the dendrites). The dendrite is relatively free from high angle grain boundaries. Also, precipitates were observed near the dendrites and in the inter-dendritic areas as shown in figure 5(a). These precipitates were recognised as η' phase ($MgZn_2$) precipitates [21]. After homogenization treatment, grains with low density dislocations were perceived as displayed in figure 5(b). SAED pattern confirms the presence of low angle grain boundaries within the grains. During homogenization treatment, majority of the precipitates which were placed in the inter-dendritic areas were almost dissolved in the aluminium matrix. After first pass, the width of the grains was reduced and shear bands were observed as shown in figure 5(c). The grains were apparently elongated along the processing direction. The width of the shear bands ranges from 1 to 1.2 μm. Also, reasonable amount of dislocation densities were observed near the grain boundaries. SAED pattern confirms that, grains are relatively free from high angle grain boundaries. Figure 5(d) presents the TEM micrograph of the alloy after second pass. In this condition, shear bands which are developed in the first pass are sliced by the shear bands formed in the second pass. Also, enhancement in the dislocation density was observed compared to previous passes. The distinct dots in the SAED pattern state that, the occurrence of low angle grain boundaries between the grains. After third pass, introduction of the deformation bands causes formation of the sub-grain boundaries as displayed in figure 5(e). Enhancement in the dislocation density was observed compared to earlier passes. The SAED pattern after third pass suggests the presence of high angle grain boundaries between the grains, although some fraction of grains having low angle grain boundaries between them was also observed. After fourth pass, due to the introduction of new deformation bands equiaxed sub-grains or cells were formed as shown in figure 5(f). High density of dislocations was observed near the sub-grain boundaries. The circular pattern in the SAED states the occurrence of large number of fine grains with high angle grain boundaries within the grains.

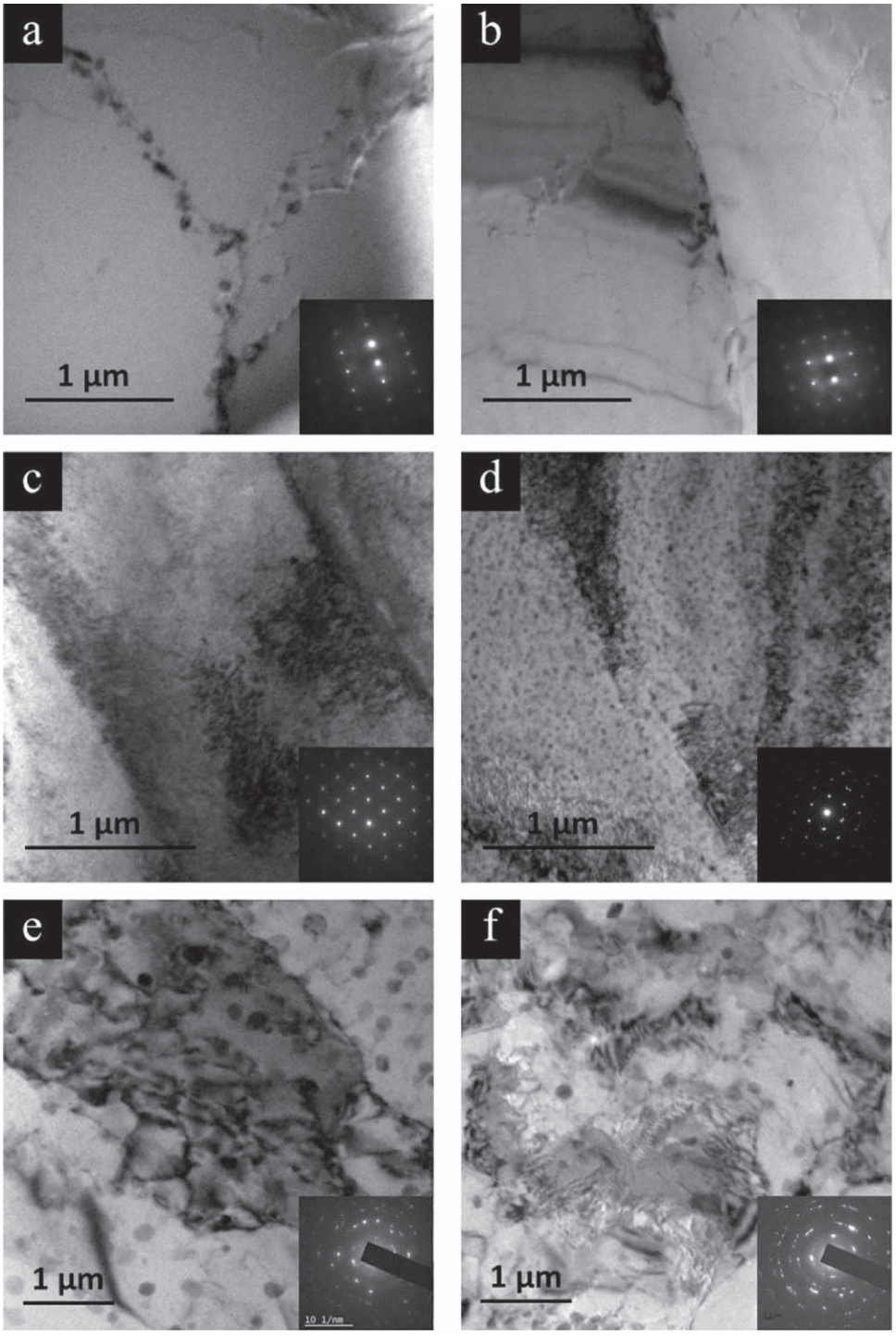

Figure 5. TEM micrographs of the A5 alloy in different conditions (a) cast, (b) homogenized, (c) 1 pass, (d) 2 pass, (e) 3 pass and (f) 4 pass.

Figure 6 presents the morphology and distribution of precipitates in the A5 alloy in different conditions. In cast condition, rod or flake shaped large quantity of $MgZn_2$ (η' phase) precipitates were observed as displayed in figure 6(a). The length of the precipitates ranges from 100 to 150 nm, the width of the precipitates ranges from 20 to 30 nm. The presence of $MgZn_2$ (η' phase) rod shape precipitates in cast condition is in consistent with earlier observations in Al 7034 cast alloy [13]. Since, after homogenization treatment, precipitates which are initially segregated along the inter-dendritic regions were almost dissolved in the aluminium matrix. Hence, secondary particles were not identified in the matrix as shown in figure 6(b). After first pass, spherical shaped precipitates were perceived as displayed in the figure 6(c) and the size of the precipitate varies from 20 to 30 nm. These precipitates were identified as intermediate metastable $MgZn_2$ (η' phase) precipitates [22]. Also, these precipitates were evenly distributed in the grains and near the grain boundaries. With increase in the number of

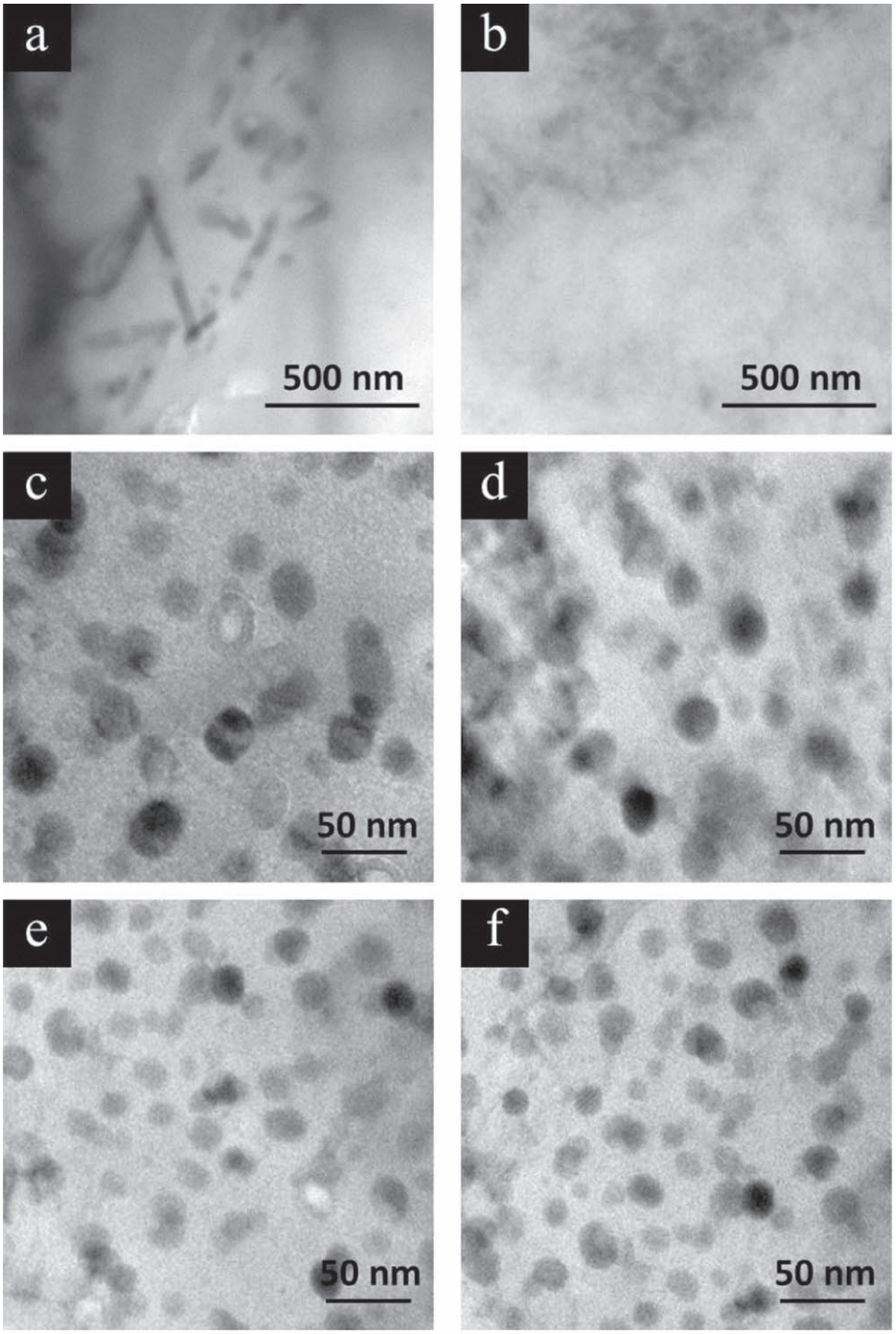

Figure 6. TEM micrographs showing the morphology and distribution of precipitates in the A5 alloy in different conditions (a) cast, (b) homogenized, (c) 1 pass, (d) 2 pass, (e) 3 pass and (f) 4 pass.

passes, the morphology of the precipitates was not changed. But, the size of the precipitates was reduced with increase in the number of passes. After second pass, the precipitate size was decreased to 20 to 25 nm as displayed in figure 6(d). After third pass, the precipitate size was reduced to 15 to 20 nm as shown in figure 6(e). After fourth pass, the precipitate size was decreased to 10 to 15 nm as presented in figure 6(f). Also, these precipitates were homogeneously distributed in the grains and nearby the grain boundaries. It is noticed that, with increase in the ECAP passes the intensity of the precipitates increased. This is due to the shearing of the η' phase ($MgZn_2$) precipitates by the introduction of dislocations in the successive ECAP passes. Also, these dislocations will acts as nucleation spots for the development of precipitates which lead to the formation of finer size spherical shaped stable $MgZn_2$ (η phase) precipitates [23].

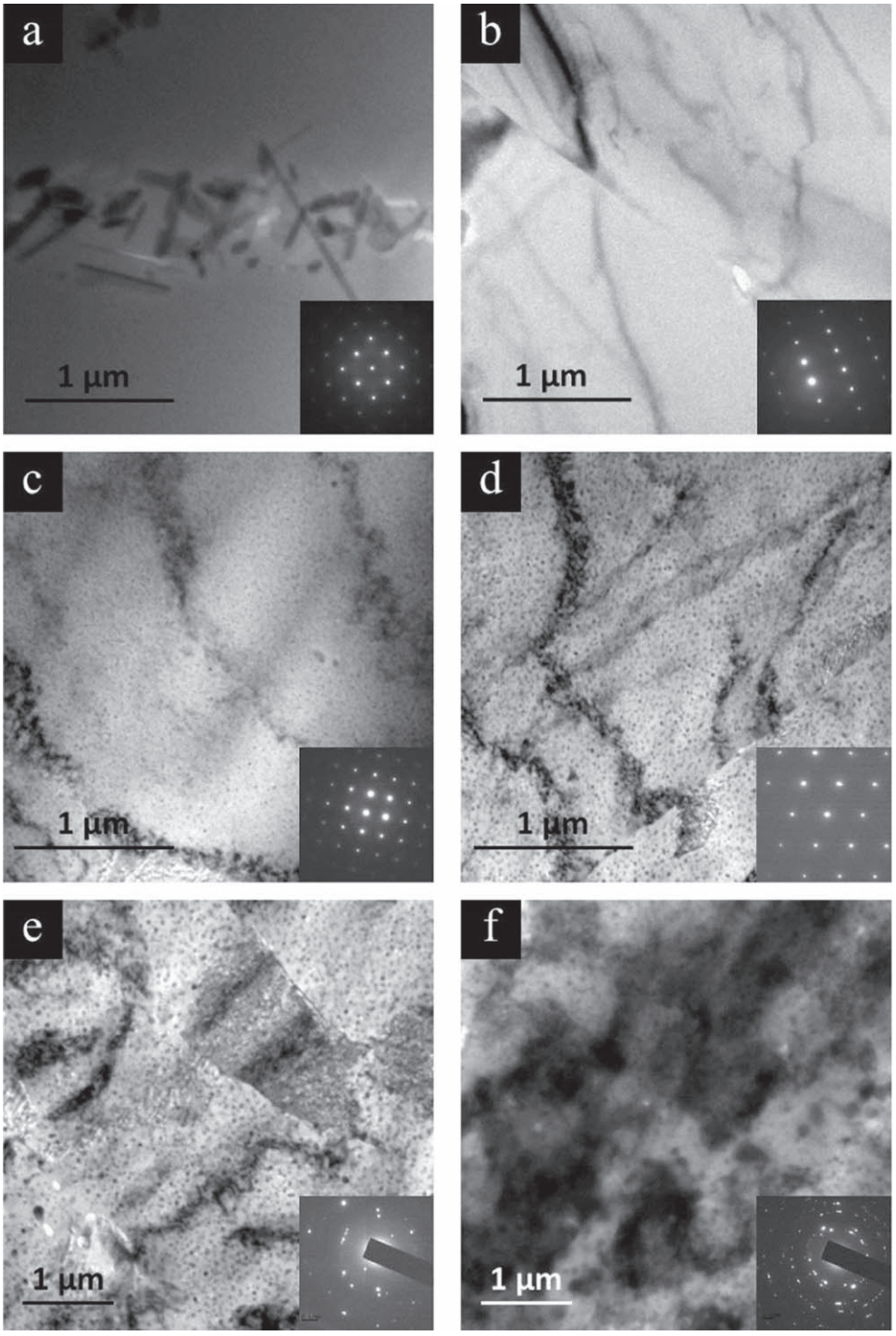

Figure 7. TEM micrographs of the A10 alloy in different conditions (a) cast, (b) homogenized, (c) 1 pass, (d) 2 pass, (e) 3 pass and (f) 4 pass.

Figure 7 presents the TEM micrographs and associated SAED patterns of the A10 alloy in different conditions. TEM micrograph of the alloy in cast condition is presented in figure 7(a), large size precipitates lying near the dendrites and inter-dendritic areas were observed. These precipitates were recognised as η' phase ($MgZn_2$) precipitates. SAED pattern included in the figure states that in cast condition presence of low angle of misorientation between the dendrites. Also, low density of intragranular dislocations was observed. Owing to the recrystallization effect during homogenization treatment, dendritic structure was replaced with large size grains as presented in figure 7(b) and precipitates present in the dendrites were almost dissolved in the matrix. In this condition, grains with low density dislocations were observed. Also, SAED pattern suggests that in the homogenized condition presence of low angle grain boundaries between the grains. Figure 7(c) presents the TEM micrograph of the A10 alloy after first pass. In this condition, elongated grains nearly parallel to the

processing direction were observed. The width of the elongated grains measured in this condition was approximately of 1 μm in size. Reasonable amount of dislocations were observed near the grain boundaries. The presence of distinct dots in the SAED pattern recommends the existence of low angle of misorientation (low angle grain boundaries) between the grains. Figure 7(d) shows the TEM micrograph of the A10 alloy after second pass. At this stage, shear bands developed during second pass cuts the elongated grains which are formed during first pass. Slight increase in the dislocation density was observed compared to first pass. SAED pattern included in the figure confirms the existence of low angle of misorientation between the grains. After third pass, few sub-grains with reasonable amount of dislocation density was observed as shown in figure 7(e). The SAED pattern after third pass confirms that most of the grains are parted by high angle grain boundaries, although presence of some fraction of grains with low angle grain boundaries was also observed. TEM micrograph of the alloy after fourth pass is displayed in figure 7(f). At this stage, equiaxed cells were observed. The equiaxed cells were formed due to the introduction of shear bands from previous passes and after fourth passes. High density of dislocations were observed near the cell boundaries. SAED pattern included in the figure states that after fourth pass existence of large volume fraction of high angle of misorientation between the cells.

Figure 8 shows the morphology and distribution of precipitates in the A10 alloy in different conditions. Figure 8(a) shows the morphology and distribution of precipitates in the A10 alloy in cast condition, rod or flake shaped $MgZn_2$ (η' phase) precipitates were perceived. The size of the precipitates observed is much bigger compared to A5 alloy. The length of the precipitates ranges from 250 to 750 nm, the width of the precipitates ranges from 50 nm to 100 nm. Increase in the size and shape of the precipitates is due to increase in the zinc quantity from 5% to 10%. Since, after homogenization treatment, precipitates which are initially segregated along the inter-dendritic regions were almost dissolved in the aluminium matrix. Hence, secondary particles were not identified in the matrix as shown in figure 8(b). After first pass, spherical shaped precipitates were perceived as displayed in figure 8(c). The size of the spherical shaped precipitates varies from 30 to 40 nm. These precipitates were identified as intermediate metastable $MgZn_2$ (η' phase) precipitates. Also, there is substantial fragmentation of the precipitates. With increase in the number of passes, the morphology of the precipitates was not changed. But, the size of the precipitates was reduced with increase in the number of passes. After second pass, the precipitate size was reduced to 20 to 30 nm as presented in figure 8(d). After third pass, the precipitate size was decreased to 15 to 25 nm as displayed in figure 8(e). After fourth pass, the precipitate size was reduced to 10 to 20 nm as shown in figure 8(f). These precipitates were identified as stable η phase precipitates Also, precipitates observed in the alloy after fourth pass were homogeneously distributed in the grains and near the grain boundaries. Reduction in the size of the precipitates is due to the shearing of the precipitates by the introduction of dislocations in the successive ECAP passes [23]. Since, ECAP processing lead to develop large amount dislocations in the material and these dislocations acts as nucleation sites for precipitate growth, large amount of spherical shaped precipitation growth had taken place at this dislocation networks.

Figure 9 presents the TEM micrographs and SAED patterns of the A15 alloy in different conditions. Figure 9(a) shows the TEM micrograph of the alloy in cast condition, large size precipitates near the dendritic regions were observed. The precipitates observed in the dendritic regions were recognised as $MgZn_2$ (η' phase) precipitates. The presence of unconnected dots in the SAED pattern of the cast sample indicates the existence of low angle of misorientation between the dendrites and low density dislocations. After homogenization treatment, large size grains with low density dislocations were perceived as displayed in the figure 9(b). Discrete spots in the SAED pattern of the homogenized sample states that, in this condition the alloy is compiled with low angle grain boundaries between the grains. During homogenization treatment, owing to the recrystallization effect dendritic structure was disappeared and majority of the precipitates existing in the dendrites were dissolved in the matrix. After first pass, elongation of the grains in the shear direction causes to form a band like structure, as displayed in figure 9(c). The width of the elongated grains was approximately equal to 1 μm. Also, noticeable amount of dislocations were observed near the grain boundaries. SAED pattern confirms that the presence of low angle grain boundaries between the grains. After second pass, due to the introduction of new shear bands wavy and ill-defined grain boundaries was perceived as shown in figure 9(d) and reasonable amount of dislocations were witnessed near the grain boundaries. The occurrence of distinct spots in the SAED recommends the occurrence of low angle of grain boundaries between the grains. After third pass, increase in the shear bands causes development of sub-grain boundaries as displayed in figure 9(e) and a large volume of dislocations especially at sub-grain boundaries were observed. The SAED pattern after third pass suggests the presence of high angle grain boundaries between the grains, although some fraction of grains having low angle grain boundaries between them was also observed. After four passes, reasonably homogenous microstructure was observed and shape of the grains is fairly equiaxed as shown in figure 9(f). High density of dislocations within the grains and near the grain boundaries was observed. The presence of rings in the SAED pattern of the fourth pass sample indicates that most of the grains are separated by high angle of misorientation (high angle grain boundaries) between them.

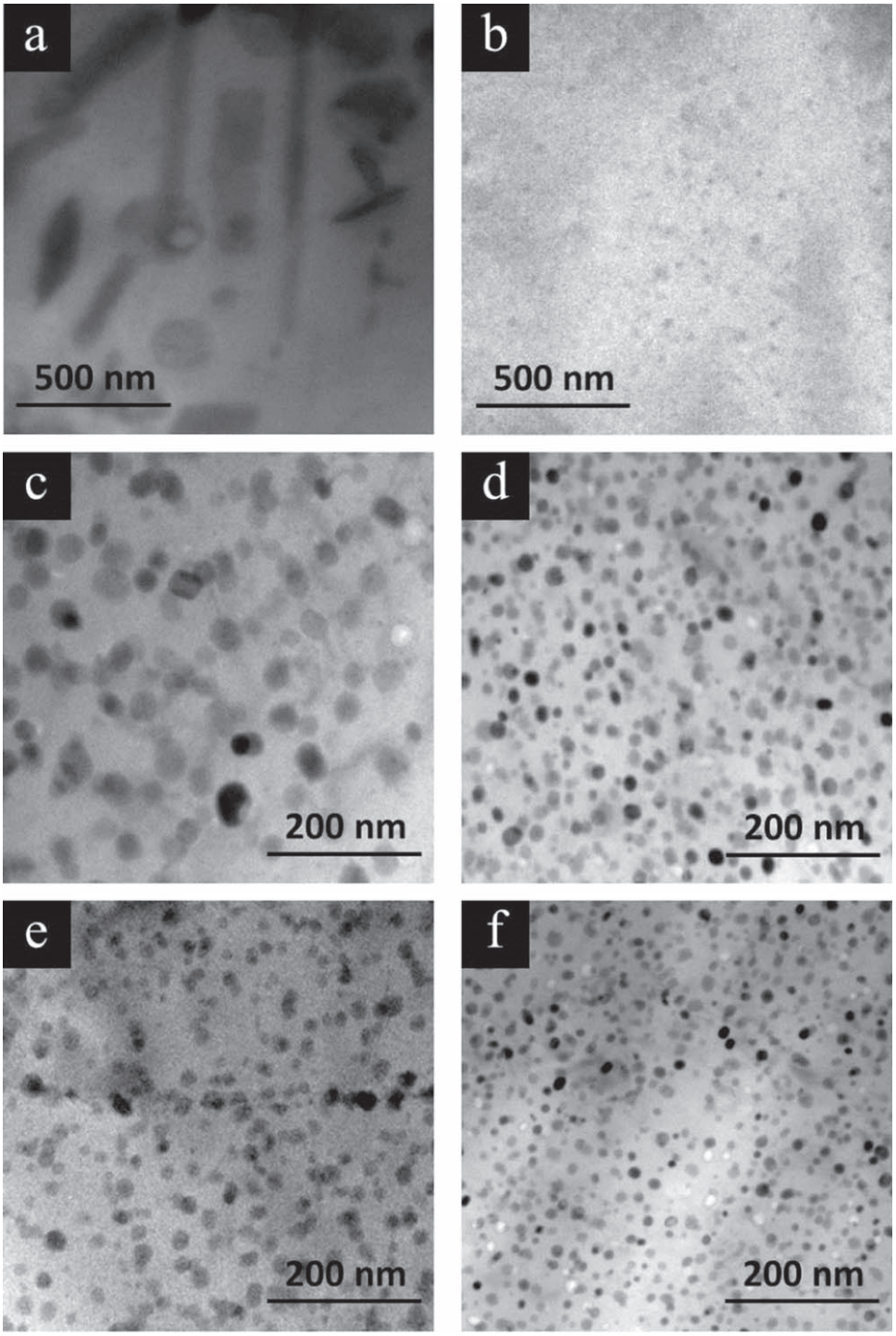

Figure 8. TEM micrographs showing the morphology and distribution of precipitates in the A10 alloy in different conditions (a) cast, (b) homogenized, (c) 1 pass, (d) 2 pass, (e) 3 pass and (f) 4 pass.

Figure 10 presents the morphology and distribution of precipitates in the A15 alloy in various conditions. Figure 10(a) presents the morphology and distribution of precipitates in the A15 alloy in cast condition, rod or flake shaped $MgZn_2$ (η' phase) precipitates were perceived. The size of the precipitates observed is much bigger compared to A5 and A10 alloy. The length of the precipitates ranges from 300 nm to 600 nm and the width of the precipitates ranges from 100 to 150 nm. Increase in the size and shape of the precipitates is due to increase in the zinc quantity to 15%. After homogenization, precipitates which are initially present the inter-dendritic regions were almost dissolved in the aluminium matrix as shown in figure 10(b). After first pass, spherical shaped precipitates were perceived as shown in figure 10(c). The size of the precipitates varies from 30 to 40 nm. These precipitates were identified as intermediate metastable $MgZn_2$ (η' phase) precipitates. With increase in the number of passes, the morphology of the precipitates was not changed. But, the size of the precipitates was

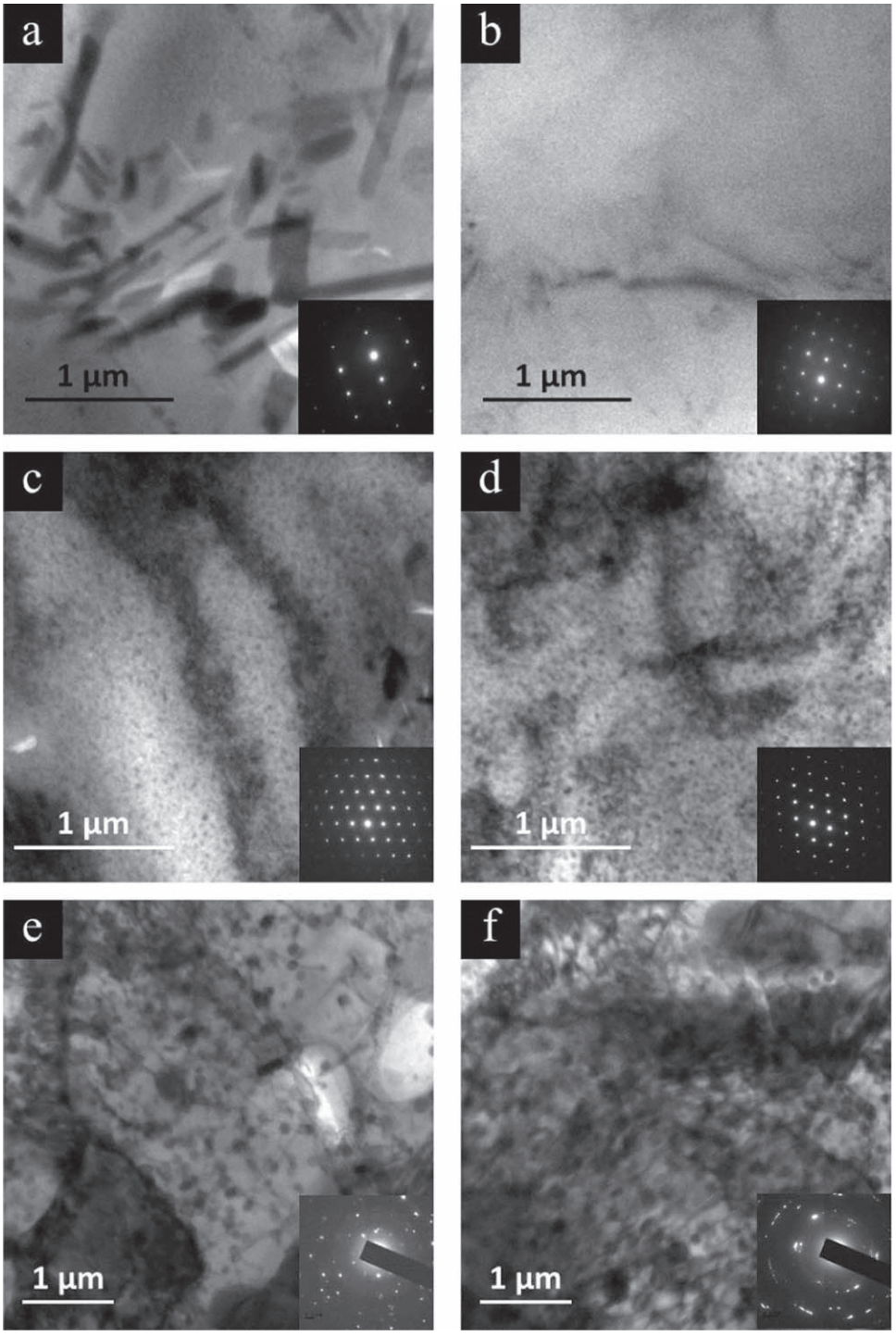

Figure 9. TEM micrographs of the A15 alloy in different conditions (a) cast, (b) homogenized, (c) 1 pass, (d) 2 pass, (e) 3 pass and (f) 4 pass.

reduced with increase in the number of passes. After second pass, the precipitate size was approximately deceased to 25 nm as shown in figure 10(d). After third pass, the precipitate size was approximately reduced to 15 nm as displayed in figure 10(e). After fourth pass, the precipitate size was approximately deceased to10 nm as presented in figure 10(f). The volume of precipitates was also enhanced with successive ECAP passes. The precipitate in this condition was identified as stable $MgZn_2$ (η phase) precipitates. Also, the precipitates observed in the alloy after fourth pass were homogeneously distributed in the grains and near the grain boundaries. Reduction in the size of the precipitates is due to the shearing of the precipitates by the introduction of dislocations in the successive ECAP passes and also new finer size precipitates growth had taken place at these dislocation tangles [23].

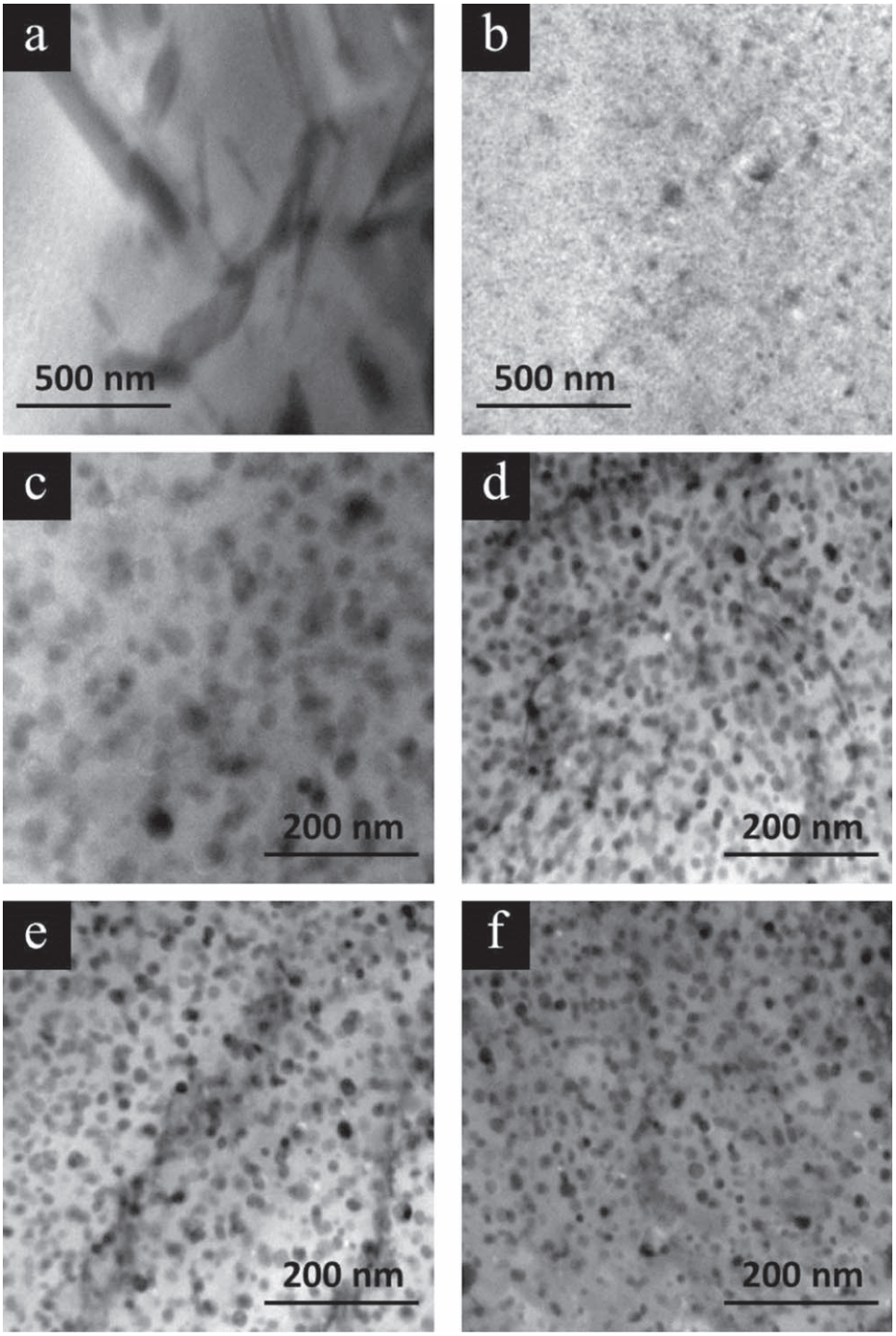

Figure 10. TEM micrographs showing the morphology and distribution of precipitates in the A15 alloy in different conditions (a) cast, (b) homogenized, (c) 1 pass, (d) 2 pass, (e) 3 pass and (f) 4 pass.

3.3. Differential scanning calorimetry (DSC)

Figure 11 shows the DSC thermographs of the A5 alloy in different conditions. In cast sample, endothermic reaction was observed at 100 to 150 °C (marked as region 1). It is owing to the dissolution of GP zones. At 200 to 250 °C (marked as region 2) exothermic reaction was observed in cast sample. It is due to the dissolution of η' phase precipitates [24]. A small shoulder (peak) at the end of the exothermic peak (marked as region 2a) at temperature 275 °C resembles to the development of η phase precipitates. Another small shoulder at 310 °C resembles to the coarsening of η phase precipitates (marked as region 2b) [25]. Again at 350 to 400 °C, endothermic reaction was observed in cast sample (marked as region 3). It is due to the dissolution of η phase precipitates [22]. Melting of the alloy takes place after 580 °C (marked as region 4). During homogenization treatment precipitates which are located in the dendritic and inter-dendritic regions are already dissolved.

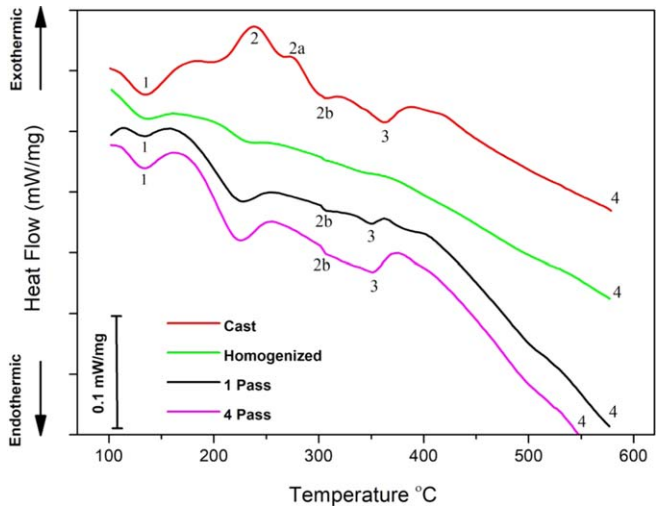

Figure 11. DSC thermographs of the A5 alloy in different conditions.

Hence, significant reactions were not observed in the homogenized sample compared to cast and ECAP processed samples. This is confirmed through TEM observations of the homogenized sample presented in figures 5(b) and 6(b). In the ECAP processed specimens, noticeable changes in the shape of the DSC thermographs were observed compared to cast sample. The first endothermic peak of the ECAP processed samples is smaller in size compared to cast sample (marked as region 1). The exothermic peak which is present in cast sample is not observed in ECAP processed samples. Since, in cast sample dissolution of GP zones and η' phase precipitates occurs nearly at the processing temperature. But, these reactions are expected to complete during initial heating for ECAP processed samples. Hence, reactions 1 and 2 in the ECAP processed samples are smaller and negligible [26]. A small shoulder at 310 °C in the ECAP processed sample (marked as region 2b) resembles to coarsening of the η phase precipitates due to the increase in the heating temperature. Endothermic reaction at 325 to 375 °C of the ECAP processed samples corresponds to the dissolution η phase precipitates. The second endothermic peak of the fourth pass sample is smaller in size compared to cast sample. This is attributed to the finer size precipitates present in the fourth pass sample. This is confirmed through TEM observations of the four pass sample presented in figure 6(f). Also, the dissolution temperature of the η phase precipitates in ECAP processed samples is 25 °C less than the cast sample. It is presumed that, the dissolution will be easier at lower temperature in the presence of fragmented and finer size precipitates [25].

Figure 12 shows the DSC thermographs of the A10 alloy in different conditions. In cast sample, low temperature endothermic reaction was observed at 125 to 150 °C (marked as region 1) corresponds to the dissolution of GP zones. Exothermic reaction at 175 to 225 °C (marked as region 2) corresponds to the dissolution η' phase precipitates. Another exothermic reaction at 250 to 280 °C (marked as region 2a) resembles the development of η phase precipitates. Shoulder at 385 °C resembles to the coarsening of η phase precipitates (marked as region 2b). High temperature endothermic reaction at 475 to 500 °C (marked as region 3) corresponds to the dissolution of the η phase precipitates. Melting of the alloy takes place after 560 °C (marked as region 4). Similar to A5 alloy, significant reactions were not observed in the homogenized sample compared to cast and ECAP processed samples. After ECAP processing, noticeable changes in the shape of the DSC thermographs were perceived. Similar to A5 alloy, low temperature endothermic reaction of the ECAP processed samples is smaller in size compared to the cast sample (marked as region 1). Also, identical to A5 alloy, exothermic reaction (resembles to the dissolution of the η' phase precipitate) is not observed in ECAP processed samples. Peak at 385 °C in the ECAP processed samples corresponds to the coarsening of the η phase precipitates (marked as region 2b). High temperature endothermic reaction of the ECAP processed samples at 475 to 500 °C (marked as region 3) corresponds to the dissolution of the η phase precipitates.

Figure 13 shows the DSC thermographs of the A15 alloy in different conditions. In cast condition, similar to A5 and A10 alloy, two endothermic peaks one at lower temperature and one at higher temperature was observed. Two exothermic peaks at intermediate temperatures were also observed. The low temperature endothermic peak at 125 to 150 °C (marked as region 1) is due to the dissolution of GP zones. Exothermic peak at 180 to 230 °C (marked as region 2) is owing to the dissolution of the η' phase precipitates. Another exothermic peak at 250 to 280 °C (marked as region 2a) corresponds to the formation of η phase precipitates. Shoulder at 435 °C (marked as region 2b) corresponds to the coarsening of η phase precipitates. High temperature endothermic peak at 470to 490 °C (marked as region 3) corresponds to the dissolution η phase precipitates. Melting of the

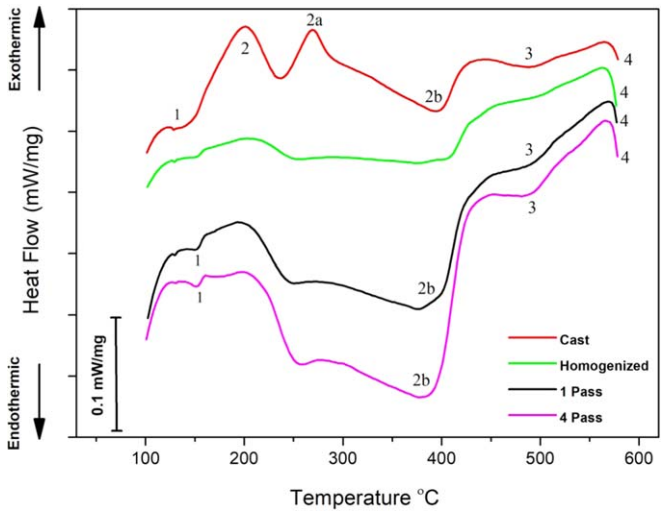

Figure 12. DSC thermographs of the A10 alloy in different conditions.

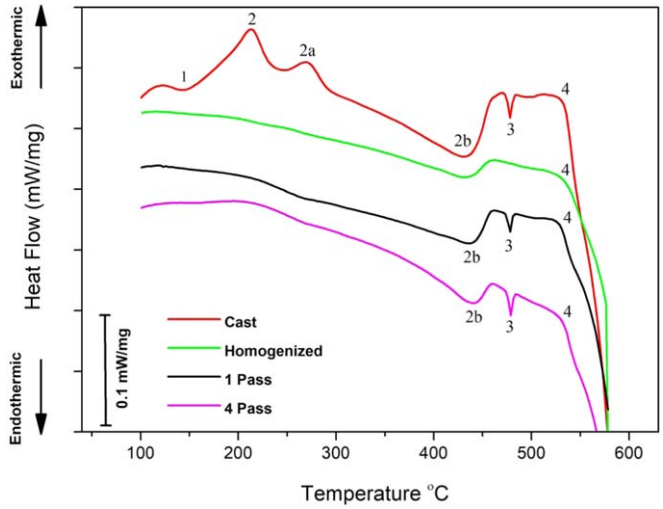

Figure 13. DSC thermographs of the A15 alloy in different conditions.

alloy takes place after 540 °C (marked as region 4). Similar to A5 and A10 alloy, significant reactions were not observed in the homogenized sample compared to cast and ECAP processed samples. After ECAP processing, noticeable changes in the shape of the DSC thermographs were observed. It is noticed that, reactions marked as 1 and 2 in the cast samples are absent in the DSC thermographs of the ECAP processed samples. Because, these reactions are expected to complete at the initial heating of the ECAP processed samples [26]. Hence, reactions 1 and 2 were not witnessed in the ECAP processed specimens. Shoulder at 440 °C in DSC thermograph of the ECAP processed specimens (marked as region 2b) corresponds to the coarsening of η phase precipitates. Endothermic peak at 470 to 490 °C (marked as region 3) corresponds to the dissolution η phase precipitates.

4. Discussion

The result from the present work confirms that ECAP processing lead to substantial decrease in the grain size of the alloys. Large volume of dislocations developed while ECAP processing promotes shearing of metastable η' phase precipitates to form stable η phase precipitates. It is noticed that, the quantity of $MgZn_2$ precipitates perceived in A10 alloy is more compared to precipitates perceived in A5 alloy. This is owing to the rise in zinc volume in the alloy form 5% to 10%. Likewise, the quantity of $MgZn_2$ precipitates perceived in A15 alloy is more compared to precipitates perceived in A10 alloy. This is owing to the rise in zinc volume in the alloy form 10% to 15%. By increasing the zinc quantity in the alloy precipitate nucleation tendency could be increased. The

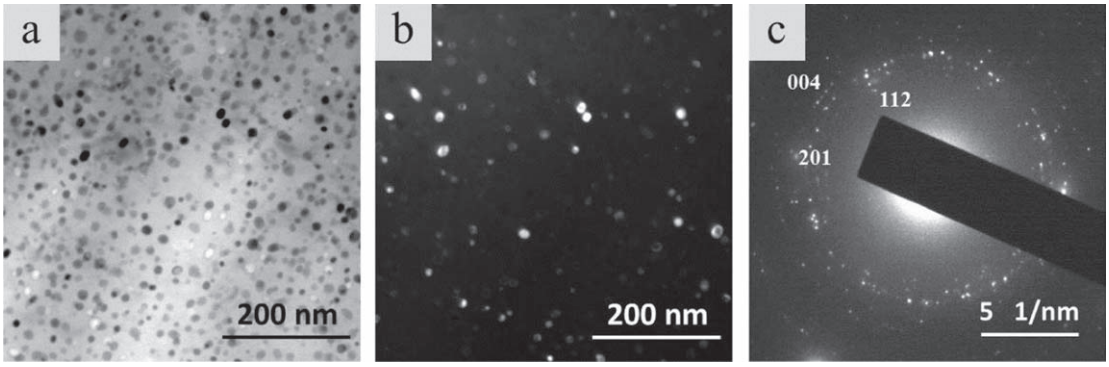

Figure 14. TEM micrographs showing the morphology and distribution of the precipitates in A10 alloy after fourth pass (a) bright field, (b) Dark field using g 112 and (c) SAED Pattern corresponding to $MgZn_2$ precipitates.

precipitation in the Al-Zn-Mg alloys is recognized to take place in the following sequence as

$$\text{Supersaturated solid solution (SSS)} \rightarrow \text{Guinier} - \text{Preston(GP) zones} \rightarrow \eta' \text{ phase (intermediate metastable)} \rightarrow \eta \text{ phase (stable)}$$

The interfacial energy between GP zones and the aluminium matrix is very less and GP zones normally forms at ambient temperature. The GP zones are coherent in nature. The intermediate metastable η' phase precipitates are semi-coherent in nature and they will form from the GP zones. The η phase precipitates are coherent in nature and these will forms from η' phase precipitates. Figure 14(a) shows the bright field TEM micrograph of the A10 alloy after four passes. It is noticed that, fine size spherical shaped precipitates were present in the alloy. For the same condition, dark field TEM micrograph is presented in figure 14(b). For the same condition, SAED pattern is presented in figure 14(c). SAED pattern suggests that particles present in the alloy correspond to $MgZn_2$ precipitates. This confirms that, after four passes, presence of equilibrium η phase ($MgZn_2$) precipitate in the alloy. Figure 15 shows the TEM-EDS analysis of the precipitates after four passes in A5, A10 and A15 alloys, respectively. EDS was carried out on both the matrix and the precipitates. It is confirmed from the EDS examination that the matrix is composed of aluminium and precipitates present in the alloy is composed of zinc and magnesium. The results stated in the present work indicate that processing through ECAP will accelerates the precipitation kinetics without altering the sequence of precipitation. Thereby showing that, processing by ECAP develops a microstructure having η precipitates without the occurrence of GP zones and η' phase precipitates by supressing the η' phase precipitates [23].

From the DSC thermographs, it is noticed that, dissolution temperature of the precipitates were reduced with successive ECAP passes. This may be owing to the presence of the finer size precipitates present in the fourth pass sample [25]. Also, the melting temperature of the alloys was reduced with rise in the zinc volume in the alloy. Since, the melting temperature of the zinc (419.5 °C) is less compared to the aluminium (661 °C). Increasing the zinc content in the alloy causes to reduce melting temperature of the alloy. It is noticed that, a small shoulder is perceived in cast sample of A5 alloy (marked as region 2a) resembles to the development of η phase precipitates. While, a bigger size peak (marked as region 2a) resembles to the development of η phase precipitates is perceived in cast sample of A10 and A15 alloy. This difference is attributed to the increase in zinc volume in the alloy. By increasing the zinc volume in the alloy precipitate nucleation tendency could be increased. Increase in the volume of the precipitates in the alloy tends to broaden the curves in the DSC thermographs. Also, shoulder corresponds to the coarsening of η phase precipitates (marked as region 2b) in A10 and A15 alloy is much bigger in size compared to the shoulder corresponds to the coarsening of η phase precipitates (marked as region 2b) in A5 alloy. Again this is owing to the rise in zinc volume in the alloy. Increase in the zinc quantity leads to increase the volume of $MgZn_2$ precipitates in the alloy. When $MgZn_2$ precipitates formation in the alloy is increased size of the shoulder also increases. It is noticed that, in all three alloys, the reactions has occurred in the following sequence as dissolution of GP zones (marked as 1) $\rightarrow$ dissolution of η' phase precipitates (marked as 2) $\rightarrow$ formation of η phase precipitates (marked as 2a) $\rightarrow$ coarsening of η phase precipitates (marked as 2b) $\rightarrow$ dissolution of η phase precipitates (marked as 3) $\rightarrow$ Melting of the alloy (marked as 4) [27]. But, temperature at which these reactions are happening is not same in all three alloys.

Table 2 displays the mechanical properties of the alloys in various conditions. In cast condition, A10 alloy possess superior mechanical properties compared to A5 alloy. This is owing to the increase in the quantity of rod or flake shaped $MgZn_2$ precipitate in A10 alloy in contrast to A5 alloy. Likewise, A15 alloy possess superior mechanical properties in contrast to the A5 and A10 alloy. This is owing to the increase in the quantity of rod or

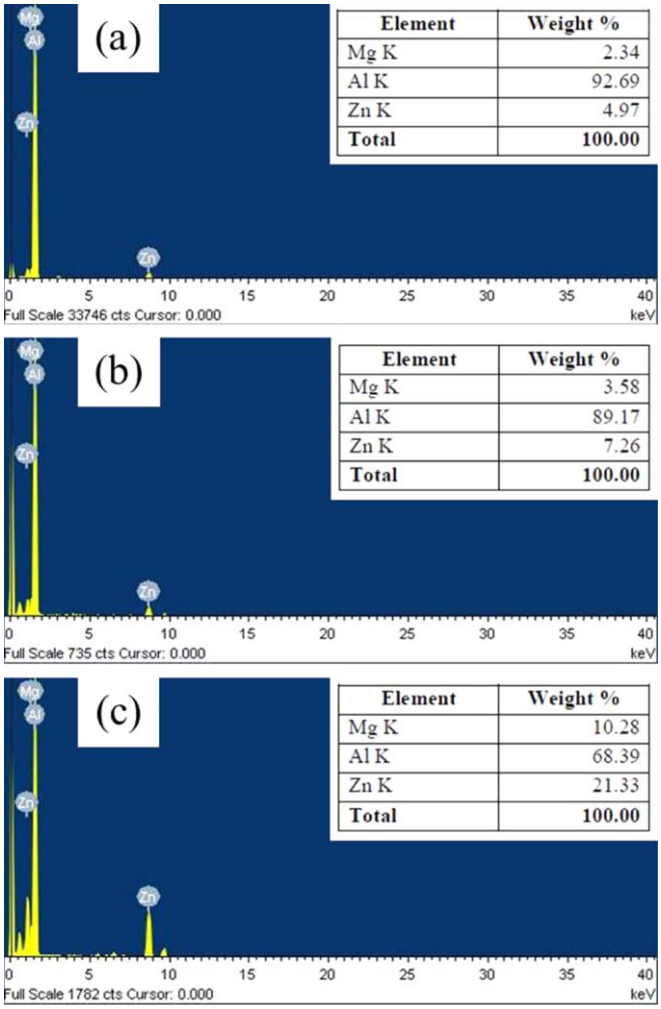

Figure 15. TEM-EDS analysis of the precipitates after four passes (a) A5 alloy, (b) A10 alloy and (c) A15 alloy.

Table 2. Mechanical properties of the alloys in different conditions.

	A5 alloy		A10 alloy		A15 alloy	
	Hardness (Hv)	UTS (MPa)	Hardness (Hv)	UTS (MPa)	Hardness (Hv)	UTS (MPa)
Cast	90 ± 8	120 ± 12	144 ± 8	140 ± 10	173 ± 7	166 ± 12
Homogenized	105 ± 8	132 ± 12	155 ± 6	156 ± 10	189 ± 6	180 ± 11
One pass	158 ± 6	218 ± 11	204 ± 6	280 ± 9	239 ± 6	340 ± 9
Two pass	175 ± 6	244 ± 9	223 ± 5	318 ± 9	261 ± 6	372 ± 7
Three pass	184 ± 6	256 ± 7	232 ± 5	342 ± 8	274 ± 5	392 ± 6
Four pass	188 ± 4	266 ± 6	240 ± 4	355 ± 6	274 ± 5	396 ± 6

flake shaped $MgZn_2$ precipitate in A15 alloy compared to A5 and A10 alloy. Increase in the quantity of $MgZn_2$ precipitate with increase in the zinc volume could be identified in the TEM micrographs presented in figures 6(a), 8(a) and 10(a). In all three alloys, marginal enhancement in the mechanical properties was perceived after homogenization treatment. But, in all three alloys, noticeable enhancement in the mechanical properties was perceived after ECAP. In all three alloys, after first pass, significant enhancement in the mechanical properties was observed in contrast to later passes. This is owing to the substantial grain refinement occurring in the first pass compared to later passes. After first pass formation of large quantity of sub-grains within the large size grains could be identified in the OM micrographs shown in figures 2(c), 3(c) and 4(c). Even after four passes, A10 alloy possess superior mechanical properties compared to A5 alloy. This is owing to the increase in the quantity of spherical shaped precipitate $MgZn_2$ precipitate in A10 alloy compared to A5 alloy which is substantially fragmented and uniformly distributed in the alloy. This could be identified in TEM micrograph shown in figure 8(f). Also, after four passes, A15 alloy possess superior mechanical properties in

contrast to the A5 and A10 alloys. This is owing to the increase in the quantity of spherical shaped precipitate $MgZn_2$ precipitate in A15 alloy in contrast to the A5 and A10 alloy which is substantially fragmented and evenly distributed in the alloy. This could be identified in TEM micrograph shown in figure 10(f). It is deduced that, along with increase in the rate of precipitation due to higher zinc content and increase in the dislocation density could be the reason for A15 alloy to possess highest mechanical properties after ECAP processing in contrast to A5 and A10 alloys.

Enhancement in the mechanical properties of the alloys after ECAP is owing to the different strengthening mechanisms. They are (a) grain refinement strengthening due to Hall-Petch effect (b) strain or work hardening of the material due to generation of high density dislocations (c) precipitation strengthening. To understand the effect of each mechanism, these mechanisms are discussed in detail.

(**a**) **Grain refinement strengthening:** In this case, coarse grains are cut by different shear bands directly into fine grains and also by the formation of high angle grain boundaries. Formation of fine grains by the intersection of shear bands could be identified in the TEM micrographs presented in figures 5(f), 7(f) and 9(f). The SAED patterns included in the TEM micrographs indicates that, misorientations across the grain boundaries are increased with increase in the number of passes.

(**b**) **Strain or work hardening effect:** The major advantage of ECAP processing is the possibility of multiple passes, so the same strain can be accumulated in each pass through the die. During processing, shear deformation will takes place. Dislocation networks formed during shearing deformation improves the strength of material. Since the moving dislocations are enforced to slice the regions of high dislocation density, with increase in the amount of strain, group of tangles gradually grows into sub-grain boundaries. With increase in the plastic strain, disorientation and sharpening of these sub-grains take place with respect to the neighbouring sub-grains.

(**c**) **Precipitation strengthening:** Since, ECAP processing lead to development of large amount dislocations in the material and these dislocations acts as nucleation sites for precipitate growth. Large amount of fine size spherical shaped precipitates growth had taken place at this dislocation networks. Also, these precipitates are homogenously distributed in the alloy. This could be clearly identified in TEM micrographs shown in figures 6(f), 8(f) and 10(f).

5. Conclusions

In the present work, experimental results are presented for precipitates evolution, thermal stability and mechanical properties of Al-Zn-Mg alloys (different compositions) subjected to ECAP processing in route B_C at 200 °C. The major outcomes of the present work are summarized as follows-

(1) In cast condition, rod or flake shaped precipitates were perceived in all three alloys and size of these rod or flake shaped precipitates were increased with increase in the zinc quantity in the alloy. After four passes, spherical shaped finer size precipitates were perceived in all three alloys and these precipitates were evenly distributed in the grains and near the grain boundaries.

(2) ECAP processing leads to development of structures having equiaxed finer grains with high density dislocations and high angle of misorientation between the grains. ECAP processing leads to accelerate the precipitation kinetics by changing the morphology of the precipitates. Both the precipitation in the alloys and formation of high angle misorientation between the grains were enhanced with increase in the ECAP passes.

(3) From the DSC analysis, it was confirmed that, through ECAP processing structure having stable η phase precipitates could be achieved without the occurrence of GP zones and intermediate η' phase precipitates. The peaks in the DSC thermographs were broadened with rise in the zinc volume in the alloy. Melting temperature of the alloys was reduced with increase in the zinc volume in the alloy.

(4) In cast condition, poor mechanical properties were perceived in all three alloys. Whereas, ECAP processing leads to achieve superior mechanical properties in all three alloys. The mechanical properties of the alloys were more influenced by first pass compared to successive ECAP passes. Both in cast condition and after 4 passes, highest mechanical properties were perceived in A15 alloy in contrast to the A5 and A10 alloys.

Acknowledgments

One of the authors Mr G K Manjunath would like to thank the Director, National Institute of Technology Karnataka and MHRD-Government of India for providing Institute Research Fellowship.

ORCID iDs

G K Manjunath https://orcid.org/0000-0001-5291-6676
K Udaya Bhat https://orcid.org/0000-0002-0752-3600

References

[1] Kutz M 2006 *Mechanical Engineers Handbook: Materials and Mechanical Design* (Hoboken, NJ: Wiley)
[2] Nandana M S, Udaya Bhat K and Manjunatha C M 2018 Effect of retrogression heat treatment time on microstructure and mechanical properties of AA7010 *J. Mater. Eng. Perform.* **27** 1628–34
[3] Zhu Y T and Langdon T G 2004 The fundamentals of nanostructured materials processed by severe plastic deformation *JOM* **56** 58–63
[4] Valiev R Z and Langdon T G 2006 Principles of equal-channel angular pressing as a processing tool for grain refinement *Prog. Mater. Sci.* **51** 881–981
[5] Segal V M 1999 Equal channel angular extrusion: from macromechanics to structure formation *Mater. Sci. Eng.* A **271** 322–33
[6] Sha G, Wang Y B, Liao X Z, Duan Z C, Ringer S P and Langdon T G 2009 Influence of equal-channel angular pressing on precipitation in an Al-Zn-Mg-Cu alloy *Acta Mater.* **57** 3123–32
[7] Cepeda-Jimenez C M, Garcia-Infanta J M, Ruano O A and Carreno F 2011 Mechanical properties at room temperature of an Al-Zn-Mg-Cu alloy processed by equal channel angular pressing *J. Alloys Compd.* **509** 8649–56
[8] Sabbaghianrad S and Langdon T G 2014 A critical evaluation of the processing of an aluminum 7075 alloy using a combination of ECAP and HPT *Mater. Sci. Eng.* A **596** 52–8
[9] Shaeri M H, Shaeri M, Salehi M T, Seyyedein S H and Djavanroodi F 2015 Microstructure and texture evolution of Al-7075 alloy processed by equal channel angular pressing *Trans. Nonferrous Met. Soc. China* **25** 1367–75
[10] Gopala Krishna K, Singh N, Venkateswarlu K and Hari Kumar K C 2011 Tensile behavior of ultrafine-grained Al-4Zn-2Mg alloy produced by cryorolling *J. Mater. Eng. Perform.* **20** 1569–74
[11] Kogtenkova O A, Mazilkin A A, Straumal B B, Abrosimova G E, Zięba P, Czeppe T, Baretzky B and Valiev R Z 2013 Phase transformations in Al-Mg-Zn alloys during high pressure torsion and subsequent heating *J. Mater. Sci.* **48** 4758–60
[12] Gopala Krishna K, Sivaprasad K, Venkateswarlu K and Hari Kumar K C 2012 Microstructural evolution and aging behavior of cryorolled Al-4Zn-2Mg alloy *Mater. Sci. Eng.* A **535** 129–35
[13] Xu C, Furukawa M, Horita Z and Langdon T G 2003 Using ECAP to achieve grain refinement, precipitate fragmentation and high strain rate superplasticity in a spray-cast aluminum alloy *Acta Mater.* **51** 6139–49
[14] DeIasi R and Adler P N 1977 Calorimetric studies of 7000 series aluminum alloys: I. Matrix precipitate characterization of 7075 *Metall. Trans.* A **8** 1177–83
[15] Starink M J and Li X M 2003 A model for the electrical conductivity of peak-aged and overaged Al-Zn-Mg-Cu alloys *Metall. Mater. Trans.* A **34** 899–911
[16] Starink M J and Wang S C 2003 A model for the yield strength of overaged Al-Zn-Mg-Cu alloys *Acta Mater.* **51** 5131–50
[17] ASM Handbook Vol 2 2001 *Properties and Selection Nonferrous Alloys and Special-Purpose Materials.* (Ohio: ASM International)
[18] Ning Z L, Guo S, Cao F Y, Wang G J, Li Z C and Sun J F 2010 Microstructural evolution during extrusion and ECAP of a spray-deposited Al-Zn-Mg-Cu-Sc-Zr alloy *J. Mater. Sci.* **45** 3023–9
[19] Chinh N Q, Jenei P, Gubicza J, Bobruk E V, Valiev R Z and Langdon T G 2017 Influence of Zn content on the microstructure and mechanical performance of ultrafine-grained Al–Zn alloys processed by high-pressure torsion *Mater. Lett.* **186** 334–7
[20] Furukawa M, Horita Z and Langdon T G 2002 Factors influencing the shearing patterns in equal-channel angular pressing *Mater. Sci. Eng.* A **332** 97–109
[21] Zhang S, Hu W, Berghammer R and Gottstein G 2010 Microstructure evolution and deformation behavior of ultrafine-grained Al–Zn–Mg alloys with fine η' precipitates *Acta Mater.* **58** 6695–705
[22] Xu C, Furukawa M, Horita Z and Langdon T G 2005 Influence of ECAP on precipitate distributions in a spray-cast aluminum alloy *Acta Mater.* **53** 749–58
[23] Gubicza J, Schiller I, Chinh N Q, Illy J, Horita Z and Langdon T G 2007 The effect of severe plastic deformation on precipitation in supersaturated Al-Zn-Mg alloys *Mater. Sci. Eng.* A **460–461** 77–85
[24] Chinh N Q, Gubicza J, Czeppe T, Lendvai J, Xu C, Valiev R Z and Langdon T G 2009 Developing a strategy for the processing of age-hardenable alloys by ECAP at room temperature *Mater. Sci. Eng.* A **516** 248–52
[25] Gao N, Starink M J, Furukawa M, Horita Z, Xu C and Langdon T G 2005 Microstructural evolution in a spray-cast aluminum alloy during equal-channel angular pressing *Mater. Sci. Eng.* A **410–411** 303–7
[26] Zhao Y H, Liao X Z, Jin Z, Valiev R Z and Zhu Y T 2004 Microstructures and mechanical properties of ultrafine grained 7075 Al alloy processed by ECAP and their evolutions during annealing *Acta Mater.* **52** 4589–645
[27] Allen R M and Vander Sande J B 1978 A high resolution transmission electron microscope study of early stage precipitation on dislocation lines in AI-Zn-Mg *Metall. Trans.* A **9** 1251–8